ingegneria sismica
International Journal of Earthquake Engineering
Anno XLIII - Num. 2 - 2026

Optimization of environmental benefits and mathematical modeling of photovoltaic-coal hybrid power generation system in low-carbon environment

Ying Liu[1,*]

[1] CHN ENERGY JIANGSU ELECTRIC POWER GROUP CO., LTD., Nanjing, Jiangsu, 210036, China

SUMMARY: *The mathematical modeling of the coal power generation model is completed by combining the relevant information in the field of coal power generation and thermal power generation, followed by the mathematical modeling of the photovoltaic power generation model by using the physical properties of the $P-N$ junction, and the photovoltaic grid-connected inverter control principle, so that the photovoltaic power generation model maintains a stable performance performance. On this basis, the PV power generation model is combined with the coal power generation model using a combination of system identification and model downscaling to obtain a hybrid PV-coal power generation system. The improvement of the standard particle swarm optimization algorithm is achieved by introducing the inertia weight way, and the solution process of the improved particle swarm optimization algorithm is supplemented, and finally an optimization model of the environmental benefits of the PV-coal hybrid power generation system based on the improved particle swarm optimization algorithm is designed. On the three test functions, the improved particle swarm algorithm outperforms the standard PSO algorithm with convergence rates of 99.21%, 97.57% and 92.68%, i.e., it verifies that the inertia weights improve the standard PSO algorithm. In addition the optimal solutions of the three objective functions are 2,077,000 yuan, 23,910,000 yuan and 235,310,000 yuan, i.e., to demonstrate the application effect of the environmental benefit optimization model of PV-coal hybrid power generation system with improved particle swarm optimization algorithm, which is of guiding value for the green sustainable development of PV-coal hybrid power generation system.*

KEYWORDS: *improved particle swarm algorithm; coal power generation model; photovoltaic power generation model; photovoltaic-coal hybrid power generation; environmental benefit optimization model*

1 Introduction

Coal power has long been used as the main power source, playing a decisive role in the security of power supply guarantee. In the long term, under the carbon neutral target, coal-fired power generation without emission reduction measures is bound to be gradually reduced or even zeroed out, but this is a long-term process that cannot be achieved overnight [1]. In the medium term, by 2030, in terms of China as a whole, coal power will still be the main power source, providing nearly 50% of electricity, as well as no less than 60% of capacity support and important grid security; as far as 2040, in terms of the contribution of electricity, coal power

*liuying19720318@126.com
https://doi.org/10.65102/is2026635
Published: 30 April, 2026

may still be the first power source variety at that time [2, 3]. Under the double constraints of low-carbon emission reduction and security of supply, on the one hand, coal power needs to be gradually transformed from a high-carbon power source to a low-carbon or zero-carbon power source, develop green and low-carbon technologies, promote the clean and efficient use of coal, and gradually withdraw from the long-term in order to comply with the economic and social development of clean and low-carbon [4-7]. On the other hand, as the security of power supply, energy system carbon neutral and ecological and environmental governance “ballast”, coal power will still be a long period of time to assume the responsibility of power security supply, from the main body of the power supply to the basic security and system regulation of the power supply, while shouldering the heat supply service [8-11]. This requires the future of coal power to more clean and low-carbon, more efficient, more flexible direction.

Thanks to technological development, the cost of photovoltaic (PV) power generation around the world has dropped dramatically over the past two decades, bringing hope for low-cost carbon emission reduction in the power system. Unlike traditional thermal power, photovoltaic equipment power production resulting in zero emissions, low carbon emission reduction oriented can significantly promote the large-scale promotion of photovoltaic power generation, through the roof photovoltaic and other distributed power generation equipment can be PV flexibly installed in residential areas or medium and low-voltage distribution network, to achieve the in situ consumption of renewable energy and the region's low carbon energy use [12-16]. However, most solar power plants have different degrees of low power factor, insufficient reactive power compensation, high harmonic content and other defects, resulting in low quality of PV power generation, and intermittency and stability deficiencies under extreme environmental disturbances [17-19]. In contrast, the reliability of traditional coal power and PV power generation are complementary and have high application value for realizing a low-carbon environment. Among them, the environmental benefits of PV-coal hybrid power generation systems are important indicators for achieving low-carbon transition and optimizing the energy consumption structure [20]. In this context, it is necessary to continuously optimize the environmental benefits of PV-coal hybrid power generation systems.

This paper starts from the relevant information in the field of coal power generation and thermal power generation, determines the main framework of the coal power generation model, which is mainly composed of four modules: the model of DEH, the model of CCS, the boiler model, and the model of the intermediate reheat turbine and generator, and designs each of the four modules in the coal power generation model. Subsequently, the mathematical model of the PV power generation model is established based on the knowledge of physical theory, and the PV grid-connected inverter control method is designed to ensure the stable performance of the PV power generation model. Through the combination of system identification and model downscaling, the coal power generation model is combined with the PV power generation model to obtain a hybrid PV-coal power generation system. Next, the objective function and constraints are set, and for the original particle swarm optimization algorithm, which has local optimum and slow convergence speed during the objective function solving process, the introduction of inertia weight is proposed to realize the improvement of the particle swarm optimization algorithm, and the corresponding solving process is also supplemented, and a PV-coal hybrid power generation system environmental benefit optimization model based on the improved particle swarm algorithm is designed at last. Finally, the model in this paper is analyzed from several aspects, aiming to verify the practical application value and effectiveness of the research content of this paper.

2 Optimized modeling of environmental benefits of PV-coal hybrid power generation system

2.1 Coal power generation model

Referring to the relevant information about coal power generation and thermal power generation field, the main framework of coal power generation model is finalized, which mainly consists of four modules: the model of DEH, the model of CCS, the boiler model, and the model of intermediate reheat turbine and generator, and the design of the four modules in the coal power generation model will be carried out in the next step.

2.1.1 Modeling of DEH

Figure 1 shows the block diagram of the DEH control system for a 600MW intermediate reheat turbine, which is mainly composed of an electric/fluid converter, an oil motor, and a controller.

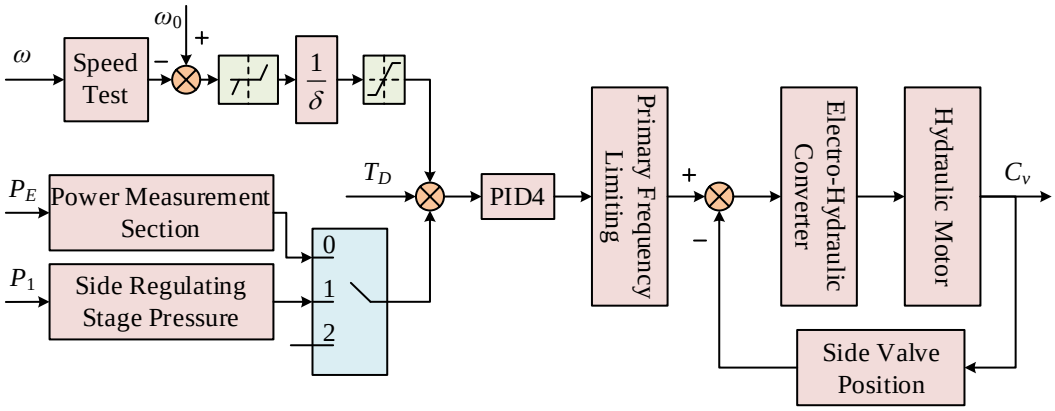

Figure 1: Gas turbine DEH control system

(1) Electro-hydraulic converter

This link will be differential voltage signal by conversion, amplification into a hydraulic signal, the hydraulic actuator to adjust the valve opening, to achieve automatic adjustment. The transfer function is as follows:

$$G_1(s) = \frac{1}{T_y s + 1} \tag{1}$$

where: T_y is the electro-hydraulic converter time constant.

(2) Oil machine

The transfer function of this link is a first order inertial link:

$$G_2(s) = \frac{1}{T_c s + 1} \tag{2}$$

where: T_c is the time constant of the oil motor.

(3) Speed feedback

The link transfer function is:

$$G_6(s)=\frac{1}{T_\omega s+1} \tag{3}$$

where: T_ω is the time constant of the speed measuring device;

(4) power feedback

When analyzing, it is assumed that the measured generator power can be completely replaced by the actual power generated by the turbine, and the link transfer function can be approximated as $G_7(s)=k$;

(5) Frequency difference amplifier

The link transfer function is:

$$G_8(s)=\frac{1}{\delta} \tag{4}$$

where: δ is the modulation factor.

2.1.2 Modeling of CCS

Figure 2 shows the coordinated control system of the machine and furnace, and the coordinated control mainly contains power regulation coupling loop, pressure regulation coupling loop, main control of steam engine and boiler, direct energy balance and boiler feed-forward control. Where: P_E is the generator power; ω_0 is the given rotational speed; ω is the actual rotational speed; P_T is the main steam pressure; P_{T0} is the given value of the main steam pressure; R is the pressure of the turbine regulating stage; T_D is the output signal of the main control of the turbine; B_D is the boiler main control output command.

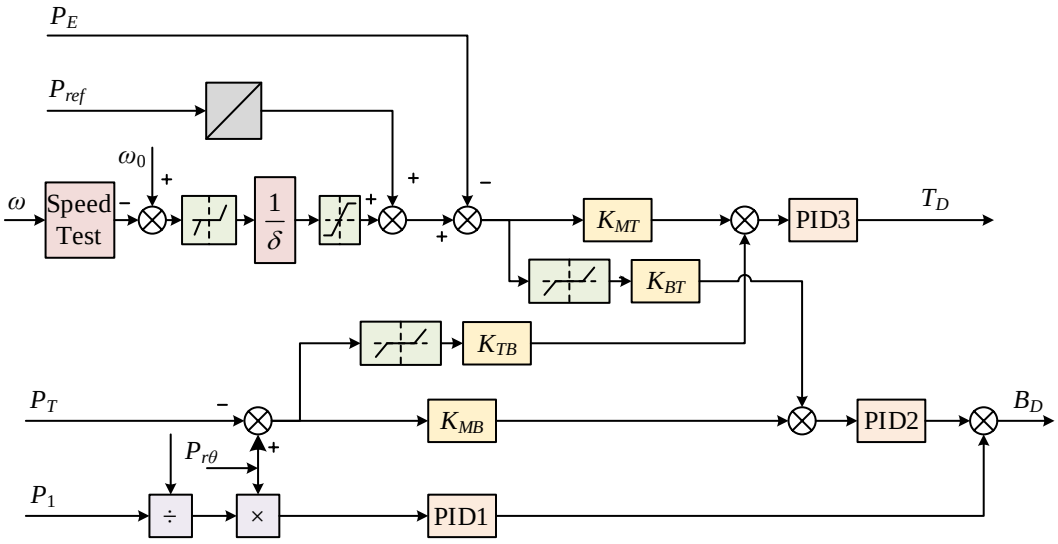

Figure 2: Model of coordinated control system for machinery and furnaces

In order to ensure the safe operation of thermal power units and to respond quickly to changes in the grid load, feed-forward-feedback control-based coordinated control is required. As shown in equation (5):

$$W = P_{T0}\frac{R}{P_T} \tag{5}$$

2.1.3 Boiler model

Figure 3 shows the boiler side of the model, the boiler section contains systems such as the pulverizing system, combustion system, turbine system, superheater system and steam busbar.

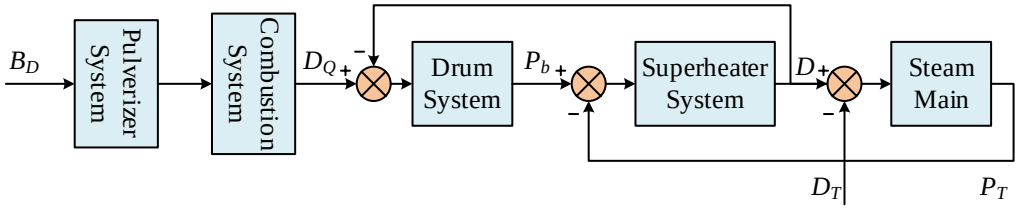

Figure 3: Block diagram of the linear model structure of the boiler

where: B_D is the coal feed control instruction; D_Q is the boiler heat absorption; p_b is the steam drum pressure; D is the boiler steam flow, P_T is the main steam pressure, and D_T is the turbine steam feed.

(1) Pulverizing system

The modeling objects of the pulverizing system include coal feeder, coal mill and primary air duct. The pure delay link shown in Eq. (6) is adopted as the transfer function model of the pulverizing system:

$$G_{10}(s) = \mathrm{e}^{-\tau s} \tag{6}$$

where: τ is the time constant of the pulverizing system.

(2) Combustion system

After the pulverizing system, the input variable is B_D and the output variable is the boiler heat absorption D_Q. The combustion and heat transfer process in the furnace can be simplified as a first-order inertial transfer function with pure delay:

$$G_{11}(s) = \frac{K_m}{T_0 s + 1} \tag{7}$$

where: T_0 is the heat transfer time constant of the combustion system; K_m is the nonlinear scaling factor;

(3) Tank system

p_b reflects the balance between D_Q and D. Considering the energy storage of the boiler steam bag, the energy balance equation of the steam bag is obtained:

$$D_Q = D + C_b\frac{dp_b}{dt} \tag{8}$$

After applying the Rasch transform to Eq. (8), the transfer function of the steam system is obtained as:

$$G_{12}(s)=\frac{p_b(s)}{D_Q(s)-D(s)}=\frac{1}{C_b s} \tag{9}$$

where: C_b is the time constant of boiler heat storage; D is the boiler steam flow rate.

(4) superheater system

Considering only the circulation characteristics of the superheater, superheater inlet pressure of p_b, superheater outlet pressure of p_T, superheater outlet and inlet pressure difference with the superheater resistance to circulation and D related to the pressure loss, the general use of flow equations, can be approximated as:

$$p_b - p_T = K_{gr} D^2 \tag{10}$$

where: K_{gr} is the pipe resistance coefficient. Equation (10) is linearized so that $R_{gr}=2K_{gr}$, R_{gr} is related to the boiler load, which increases with the load, and its differentiation is followed by the Rasch transform of equation (10) to obtain the transfer function as:

$$G_{14}(s)=\frac{\Delta D(s)}{\Delta p_b(s)-\Delta p_T(s)}=\frac{1}{R_{gr}} \tag{11}$$

(5) Steam parent pipe

P_T is taken as the output variable, and the difference between D and D_T is taken as the input variable, from which the differential equation for steam energy transfer in piping is obtained as:

where: C_M is the heat storage coefficient of the steam pipe.

The Raschel transformation of equation (11), the transfer function is obtained as:

$$G_{15}(s)=\frac{P_T(s)}{D(s)-D_T(s)}=\frac{1}{C_M s} \tag{12}$$

2.1.4 Modeling of intermediate reheat turbines and generators

The turbine and generator system is shown in Figure 4. This section contains two main parts: the turbine and the generator, and the turbine is composed of a steam volume and an intermediate reheat turbine.

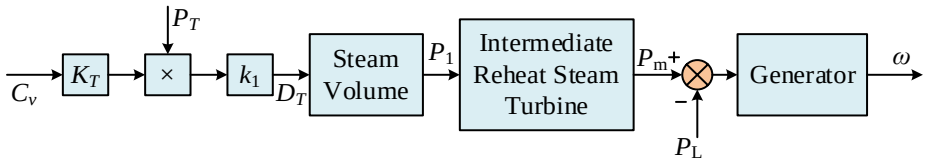

Figure 4: Steam turbine and generator system

(1) The steam flow rate of the turbine

D_T is a function of P_T and C_v, and the resistance of the steam-using equipment is:

$$\frac{1}{R_T} = K_T C_v \tag{13}$$

The transfer function of the turbine steam intake is:

$$D_T(s) = k_1 P_T \frac{1}{R_T} \tag{14}$$

where: C_v is the valve opening; K_T is the proportionality coefficient corresponding to the turbine regulating valve opening and the actual load; k_1 is the proportionality coefficient corresponding to the turbine regulating valve opening and the steam flow.

(2) Steam volume

The transfer function of the steam chamber volume can be expressed by the first-order inertia link shown in equation (15):

$$G_3(s) = \frac{1}{T_\rho s + 1} \tag{15}$$

where: T_ρ is the vapor volume time constant.

(3) Intermediate Reheat Turbine

The intermediate reheat turbine can be described by the parallel connection of proportional and inertial links to characterize its power:

$$G_4(s) = C_B + \frac{C_H}{T_H s + 1} \tag{16}$$

where: C_B for the intermediate reheat unit high-pressure cylinder power accounted for the proportion of the total power, generally take 1 / 3; C_H for the intermediate reheat unit in the low-pressure cylinder power accounted for the proportion of the total power, generally take $2/3\left(C_B + C_H = 1\right)$; T_H for the intermediate reheat volume time constant.

(4) generator

a) generator stand-alone operation, can be expressed by the formula (17):

$$G_5(s) = \frac{1}{T_a s} \tag{17}$$

b) For grid-connected operation, the turbine-generator unit can be represented by equation (18):

$$G_5'(s) = \frac{1}{T_a s + \beta} \tag{18}$$

where: T_a is the generator rotor time constant. β is the self-balancing coefficient. Since the frequency control of the whole generation system will be studied in this paper, the grid-connected operation model as shown in equation (18) will be used in this paper.

2.2 Modeling of photovoltaic power generation

After completing the design work of the coal power generation model, the mathematical model of the photovoltaic power generation model is constructed according to the physical properties of the $P-N$ junction, and the control principle of the photovoltaic grid-connected inverter is also given in detail, aiming to ensure that the photovoltaic power generation model has a stable performance.

2.2.1 Mathematical modeling of photovoltaic power generation models

Based on the physical properties of the $P-N$ junction, the dual diode model of a photovoltaic cell is shown in Fig. 5. In this model, the diode D_1 can be used to equate the recovery current between the P region and the N region due to the movement of the oligon. The diode D_2 can be used to equate the recovery motion of the oligon in the depletion layer due to energy excitation.

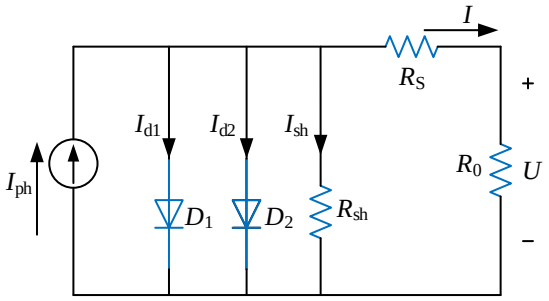

Figure 5: Dual diode model of photovoltaic cells

The simplified equivalent model of photovoltaic power generation model is shown in Fig. 6, ignoring the diode D_2, the simplified equivalent model of photovoltaic cell can be obtained.

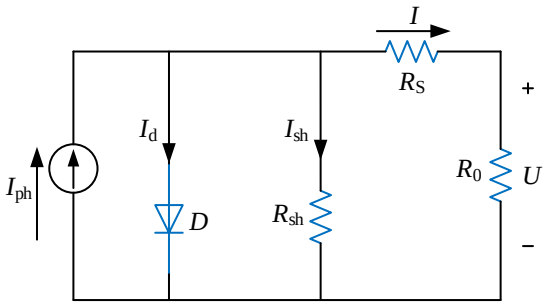

Figure 6: The photovoltaic power generation model simplifies the equivalent model

The mathematical relationship between the output current and output voltage of the PV model can be obtained:

$$I = I_{ph} - I_0\left[\exp\left(\frac{q(U+R_sI)}{KTA}\right)-1\right]-\frac{U+R_sI}{R_{sh}} \tag{19}$$

Among them:

$$I_D = I_0\left[\exp\left(\frac{q(U+R_sI)}{KTA}\right)-1\right] \tag{20}$$

$$I_{sh} = \frac{U+R_sI}{R_{sh}} \tag{21}$$

where: I is the photovoltaic current; U is the photovoltaic voltage; I_{ph} is the photogenerated current; I_0 is the reverse saturation current of the photovoltaic, which is generally a constant; A is the curvilinear constant of the P-N junction of the photovoltaic, which takes the value range of 1~5; R_{sh} is the equivalent shunt resistance of the photovoltaic cell; R_s is the equivalent series resistance of the photovoltaic; and K is the Boltzmann constant $\left(1.38\times10^{-13}\ J/K\right)$;

q is the unit charge $\left(1.6\times10^{-19}\mathrm{C}\right)$; T is the absolute temperature of the PV power model.

Eqs. (19)~(21) are analytical expressions obtained according to the physical principles of the PV power generation model, which are mainly used to theoretically analyze the characteristics of the PV power generation model, and the parameters in the expressions, I_{ph}, I_0, R_{sh}, A, are related to the operating temperature and the intensity of the solar radiation, which makes it difficult to determine the magnitude of their values. In practical engineering applications, the analytical expression of the PV model is usually used for engineering derivation.

In general, since R_{sh} is very large and R_s is very small, both of them are negligible with $I_{ph}\approx I_{sc}$, then Eq. (19) can be simplified as:

$$I = I_{sc}\left\{1-C_1\left[\exp\left(\frac{U}{C_2U_{oc}}\right)-1\right]\right\} \tag{22}$$

where: $C_1 = I_0/I_{sc}$; $C_2 = 1\Big/\ln\left(\frac{1}{C_1}+1\right)$; and I_{sc} and U_{oc} are the short-circuit current and the open-circuit voltage measured under the standard test conditions, respectively.

Based on the voltage value U_m and current value I_m corresponding to the maximum power point of the PV cell, C_1 and C_2 can be derived:

$$C_1 = \left(1-\frac{I_m}{I_{sc}}\right)\exp\left(\frac{-U_m}{C_2U_{oc}}\right) \tag{23}$$

$$C_2 = \frac{\left(\frac{U_m}{U_{oc}}-1\right)}{\ln\left(1-\frac{I_m}{I_{sc}}\right)} \tag{24}$$

Eqs. (22)~(24) are the practical mathematical model of PV power generation model, only provide the parameters of PV power generation model under standard test conditions: I_{sc}, U_{oc}, I_{m} and U_{m}, then we can get the volt-ampere characteristic curves of the PV power generation model under the standard test conditions, take $S_{\mathrm{ref}}=1000\mathrm{W/m}^2$ as the reference solar radiation intensity, $T_{\mathrm{ref}}=25^{\circ}\mathrm{C}$ as the reference battery temperature, and the model is corrected according to the actual radiation intensity and temperature. The relationship between ambient temperature T_{air} and temperature T is:

$$T=T_{air}+0.03S \tag{25}$$

In the formula, S represents the solar radiation intensity. Based on the reference radiation intensity and I_{sc}, U_{oc}, U_{m} and I_{m} at the reference temperature, the new radiation intensity and I'_{sc}, U'_{oc}, I'_{m} and U'_{m} at the temperature of the power generation model can be calculated. Then, substituting them into the practical expression, the new voltage-current characteristic curve at the new radiation intensity and temperature can be obtained. That is:

$$\begin{cases}\Delta T=T-T_{ref}\\ \Delta S=S/S_{ref}-1\\ I'_{sc}=I_{sc}(\Delta S+1)(1+a\Delta T)\\ U'_{oc}=U_{oc}(1-c\Delta T)\ln(1+b\Delta S)\\ I'_{m}=I_{m}(\Delta S+1)(1+a\Delta T)\\ U'_{m}=U_{m}(1-c\Delta T)\ln(1+b\Delta S)\end{cases} \tag{26}$$

where: typical values of coefficients a, b and c are $a=0.0025/^{\circ}\mathrm{C}$, $b=0.5$ and $c=0.00288/^{\circ}\mathrm{C}$.

Eq. (26) is the mathematical model of the single photovoltaic power generation model. In practice, a number of single photovoltaic cells encapsulated to form a photovoltaic power generation model components, a certain number of photovoltaic cell components through the series-parallel combination of photovoltaic arrays. Therefore, the mathematical expression of the PV array can be easily obtained from the mathematical model of the single PV power generation model, and only the scaling of each power quantity of the PV power generation model assembly is required, i.e., the voltage is multiplied by the number of series connections, and the current is multiplied by the number of parallel connections.

2.2.2 PV Grid-tied Inverter Controls

The grid-connected PV power generation system mainly consists of a PV cell array, a Boost DC converter circuit, a voltage-type three-phase bridge-type grid-connected inverter, an LC-type filter, as well as a collector line and a transformer. The structure of the PV grid-connected inverter system in the dq coordinate system is shown in Fig. 7, and Fig. 8 shows the block diagram of the double closed-loop overall control of the PV grid-connected inverter. Taking the currents i_{La}, i_{Lb}, i_{Lc} of the filter inductor and the voltages u_{oa}, u_{ob}, u_{oc} of the filter capacitor as the state quantities, under the system equilibrium condition and according to Kirchhoff's theorem, the mathematical model of the grid-connected PV inverter system in the three-phase static coordinate system can be expressed as:

$$L\begin{bmatrix}\frac{di_{La}}{dt}\\ \frac{di_{Lb}}{dt}\\ \frac{di_{Lc}}{dt}\end{bmatrix}=\begin{bmatrix}u_{ia}\\ u_{ib}\\ u_{ic}\end{bmatrix}-\begin{bmatrix}u_{oa}\\ u_{ob}\\ u_{oc}\end{bmatrix} \tag{27}$$

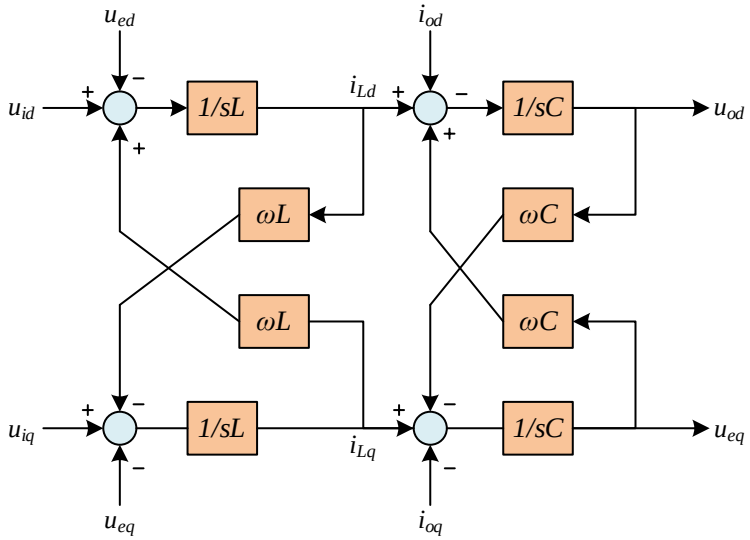

Figure 7: Photovoltaic grid-connected inverter system

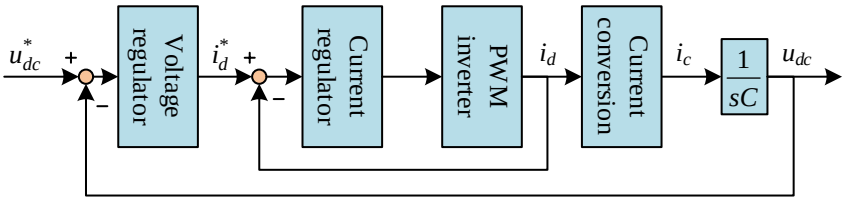

Figure 8: Overall control block diagram of grid-connected inverter

The block diagram of the current inner loop control is shown in Fig. 9. In the figure, $G_{\mathrm{PWM}}(s)$ is the transfer function of the inverter bridge, and its amplification characteristic has a proportional gain K_{PWM} indicated when the switching frequency is high enough. $G_a(s)$ is the filter transfer function.

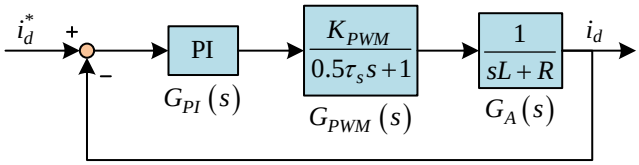

Figure 9: Current inner loop control block diagram

The block diagram of the DC voltage outer-loop control structure of the PV grid-connected inverter is shown in Fig. 10, and the key is the solution of the transfer function between the

current inner-loop output current i_{d} and the DC capacitor input current i_{dc}.

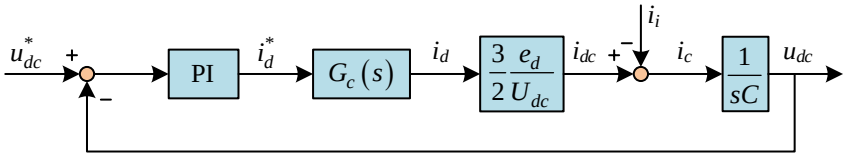

Figure 10: Block diagram of the outer loop control for the DC side voltage

In the figure: $G_{\mathrm{c}}(s)$ is the closed-loop transfer function of the current inner-loop equivalent; i is the output current of the DC capacitor; i_{c} is the dynamic current of the DC capacitor, and $i_{\mathrm{c}} = i_{\mathrm{dc}} - i$. According to the power conservation relation, $P = i_{dc}u_{dc} = \frac{3}{2}e_d i_d$, which can be obtained as follows: $i_{dc} = \frac{3e_d i_d}{2u_{dc}}$, and $u_{\mathrm{dc}} = U_{\mathrm{dc}}$ at steady state, which leads to the transfer relation in Fig.

2.3 PV-Coal Hybrid Power Generation System

To facilitate the following coal power generation model analysis work to carry out, and coal power generation model named DEH-CCS, combined with the above coal power generation model and photovoltaic power generation model, the design of the PV-coal hybrid power generation system, PV-coal hybrid power generation system is shown in Figure 11. Based on the PV-coal primary FM model contains three thermal power plants, a PV power plant and the grid, so this paper will identify the PV-coal hybrid power generation system in three pieces, i.e., PV arrays connected to the grid, and ultimately use the simplified model obtained from the identification to build the overall simplified model of the system. The PV-coal hybrid power generation system mainly contains a PV power generation model, a coal power generation model, a power grid model and a primary frequency control loop of thermal power units, where S_i is the light intensity of the i th PV system, T_i is the temperature of the i th PV system, P_{pv_i} is the active power of the i th PV system, and P_{pv_total} is the total active power of the PV system, P_{ref_i} is the power given reference value of the i th thermal unit, P_{m_i} is the output power of the i th thermal unit, P_{m_total} is the total active power of the coal generation model, P_L is the power of the load, and f is the frequency of the PV-coal hybrid frequency of the power generation system.

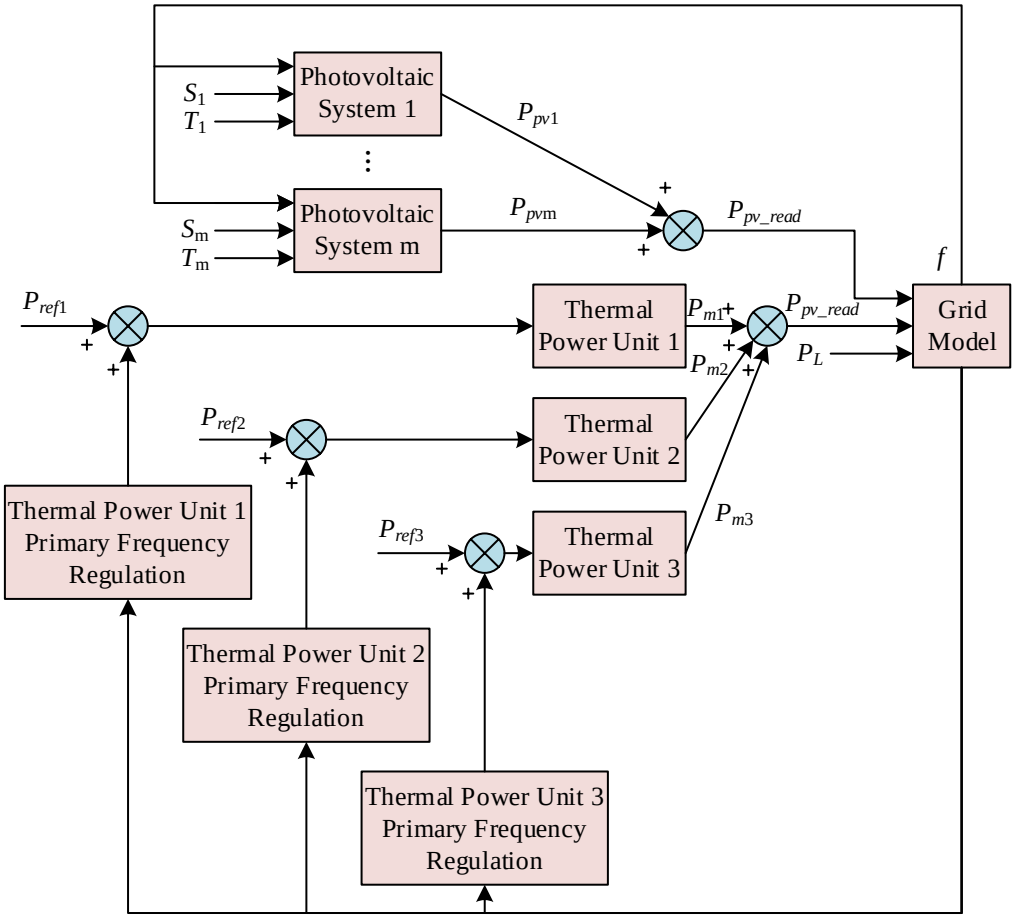

Figure 11: Photovoltaic-coal hybrid power generation system

2.4 Environmental Benefit Optimization Model

On the basis of photovoltaic-coal hybrid power generation system, three objective functions and five constraints are determined, and for the original particle swarm optimization algorithm, which has local optimum and slow convergence speed during the objective function solving process, it is proposed to introduce the inertia weight to realize the improvement of the particle swarm optimization algorithm, and at the same time, it also supplements the corresponding solving process, and finally completes the construction of the optimization model of the environmental benefits of the photovoltaic-coal hybrid power generation system. The optimization model of environmental benefits of PV-coal hybrid power generation system is finally constructed.

2.4.1 Objective function

In this paper, the minimization of the sum of the power generation cost C_{DG} and the grid line active loss cost C_{loss}, and the environmental benefit C_{ee} is taken as the objective model for the optimal configuration of the PV-coal hybrid power generation system, and the expression can be written as:

$$\min Z = C_{DG} + C_{loss} - C_{ee} \tag{28}$$

where Z is the objective function value of the sum of power generation cost, line active loss cost, and environmental benefits of the PV-coal hybrid power generation system.

(1) Investment and operation cost of PV-coal hybrid power generation system C_{DG}:

$$C_{DG} = \sum_{i=1}^{n} \tau_{\max i} P_{DG,i} C_{k,i} \tag{29}$$

where: $\tau_{\max i}$ is the annual maximum load utilization hours of the i th PV-coal hybrid power generation system, $P_{DG,i}$ is the installed active capacity of the i th PV-coal hybrid power generation system, $C_{k,i}$ is the generation cost per unit of power of the i th PV-coal hybrid power generation system, and n is the number of PV-coal hybrid power generation systems.

(2) Line active loss cost C_{loss}:

$$C_{loss} = \sum_{k=1}^{N} \tau_{\max k} C_e R_k \left(\frac{P_k}{U_N \lambda_k} \right)^2 \tag{30}$$

In the formula: $\tau_{\max k}$ represents the annual maximum loss time of the k th branch, C_e is the unit electricity price, R_k is the resistance of the k th branch, U_N is the rated voltage of the power grid, λ_k is the load power factor on the k th branch, P_k is the active power of the k th branch, and N is the number of branches.

(3) Environmental benefits of PV-coal hybrid power generation system C_{ee}

When optimizing the configuration of PV-coal hybrid power generation system, it is necessary to consider its environmental benefits, and its maximum benefit function can be expressed as follows:

$$C_{ee} = \max \left[\left(\sum_{i=1}^{4} (\alpha_i + \beta_i) q_{1,i} \times 10^{-3} + 1.4 \sum_{i=1}^{6} \frac{q_{2,i} \times 10^{-6}}{\gamma_i} \right) \times \sum_{i=1}^{n} \tau_{\max i} \times P_{DG,i} \right] \tag{31}$$

2.4.2 Constraints

(1) Power balance constraints:

$$\begin{cases} P_{Gi} - U_i \sum_{j=1}^{N} U_j \left(G_{ij} \cos \delta_{ij} + B_{ij} \sin \delta_{ij} \right) = 0 \\ Q_{Gi} - U_i \sum_{j=1}^{N} U_j \left(G_{ij} \cos \delta_{ij} - B_{ij} \sin \delta_{ij} \right) = 0 \end{cases} \tag{32}$$

where: P_{Gi} and Q_{Gi} are the active and reactive power injected at node i, respectively; U_i and U_j are the voltage amplitudes at nodes i and j, respectively, δ_{ij} is the phase angle difference between nodes i and j, G_{ij} is the branch conductance, and B_{ij} is the branch denona.

(2) Node voltage constraints:

$$U_{\min,i} < U_i < U_{\max,i} \tag{33}$$

where $U_{\min,i}$ and $U_{\max,i}$ are the upper and lower voltage limits of node i, respectively, and its penalty function is expressed as:

$$K(U_i) = \begin{cases} k_u\left(U_{\min,i} - U_i\right), & U_i < U_{\min,i} \\ k_u\left(U_i - U_{\max,i}\right), & U_i > U_{\max,i} \\ 0 \qquad\qquad\quad , & U_{\min,i} < U_i < U_{\max,i} \end{cases} \tag{34}$$

where k_u is the penalty factor for node voltage deviation from the operating limit, which is generally taken to be a very large positive constant, or 0 when the voltage does not cross the limit.

(3) Nodal current constraint:

$$0 < I_k \le I_{k,\max} \tag{35}$$

where $I_{\mathrm{k,max}}$ is the maximum branch current allowed to pass through the branch, and its penalty function is expressed as:

$$K_I(I_k) = \begin{cases} k_I\left(I_k - I_{k,\max}\right) & I_k \ge I_{k,\max} \\ 0 & I_k < I_{k,\max} \end{cases} \tag{36}$$

where K_I is the line current overrun penalty factor, which is generally taken to be a very large positive constant and 0 when the current is not overrun.

(4) Node capacity constraint:

$$0 < P_{DG,i} < P_{DG\max,i} \tag{37}$$

where $P_{DG\max,i}$ is the maximum capacity allowed to be installed at the i th node, and its penalty function is expressed as:

$$K(P_{DG}) = \begin{cases} k_p\left(P_{DG,i} - P_{DG\max,i}\right) & P_{DG,i} \ge P_{DG\max,i} \\ 0 & P_{DG,i} < P_{DG\max,i} \end{cases} \tag{38}$$

where k_p is the node i access capacity overrun penalty factor, which is generally taken to be a very large positive constant and 0 when the capacity is not overrun.

(5) Total capacity constraint:

$$\sum_{i=1}^{n} P_{DG,i} \le 0.25 P_L \tag{39}$$

where P_L is the total active load of the grid and $\sum_{i=1}^{n} P_{DG,i}$ is the total active capacity of the

installed PV-coal hybrid generation system, which is expressed as a penalty function:

$$K(P_{DG,i})=\begin{cases} k\left(\sum_{i=1}^{n}P_{DG,i}-0.25P_L\right) & \sum_{i=1}^{n}P_{DG,i}\geq 0.25P_L \\ 0 & \sum_{i=1}^{n}P_{DG,i}<0.25P \end{cases} \tag{40}$$

Therefore, after adding the penalty function of the constraints, the objective function of the optimization becomes:

$$\begin{aligned} \min Z=&\sum_{i=1}^{n}\tau_{\max,i}P_{DG,i}C_{k,i}+C_e\sum_{k=1}^{N}\tau_{\max,k}R_k\frac{P_k^2}{U_N^2\lambda_k^2} \\ &-\left[\left(\sum_{i=1}^{4}(\alpha_i+\beta_i)q_{1,i}\times10^{-3}+1.4\sum_{i=1}^{6}\frac{q_{2,i}\times10^{-6}}{\gamma_i}\right)\right. \\ &\left.\times\sum_{i=1}^{n}\tau_{\max,i}\times P_{DG,i}\right]+\sum_{i=1}^{n}K(U_i)+\sum_{k=1}^{N}K_I(I_k) \\ &+\sum_{i=1}^{n}K(P_{DG})+K(P_{DG,i}) \end{aligned} \tag{41}$$

The principle followed in the rational configuration of PV-coal hybrid power generation system can be summarized as follows: under the condition of satisfying the capacity, voltage and current constraints, to minimize the investment and operation cost of PV-coal hybrid power generation system, to minimize the cost of active network loss of the line, and to maximize the environmental protection benefit of PV-coal hybrid power generation system.

2.4.3 Improved particle swarm optimization algorithm

Let the solution space be D-dimensional and the total number of particles be N, the best position searched by an individual is called the individual extreme point p_{id}^{best}, and the best position searched by the group is called the global extreme point p_{gd}^{best}. Each particle keeps updating its velocity and position through the two extreme points p_{id}^{best} and p_{gd}^{best}, approaching the position of the optimal solution one by one. The position of the ith particle is denoted by $x_{id}(t)$, and the velocity and direction of the particle movement is denoted by the velocity $v_{id}(t)$, and the transformation of the particle's position is determined by the joint decision of its own current position and the particle's velocity, which can be expressed as follows:

$$x_{id}(t)=x_{id}(t-1)+v_{id}(t)\quad i=1,2,...,N\quad d=1,2,...,D \tag{42}$$

$$\begin{aligned} v_{id}(t)=&v_{id}(t-1)+C_1\times rand_1\times\left(p_{id}^{best}-x_{id}(t)\right) \\ &+C_2\times rand_2\times\left(p_{gd}^{best}-x_{id}(t)\right) \end{aligned} \tag{43}$$

where: $x_{id}(t)$ is the d-dimensional component of the current position of particle i in the t th iteration; $v_{id}(t)$ is the d-dimensional component of the current velocity of particle i in

the tth iteration; N is the size of the population of particles, and the size of the range varies depending on the situation; $rand_1$, $rand_2$ are the random numbers uniformly distributed in the range between $[0,1]$ random numbers; p_{id}^{best} is the d-dimensional component of the individual pole position of particle i; p_{gd}^{best} is the d-dimensional component of the global pole position of the whole population; C_1, C_2 are the learning factors, constant and non-negative, respectively regulate the maximum step of evolution in the p_{id}^{best} and p_{gd}^{best} directions; $x_{id} \in [-x_{\max,d}, x_{\max,d}]$, $v_{id} \in [-v_{\max,d}, v_{\max,d}]$, which sets the range of particle positions and velocities, prevents the particle swarm algorithm from searching blindly.

In order to improve the convergence speed of the elementary particle swarm algorithm, inertia weights are introduced for the first time, i.e., an inertia weight ω is added for the evolutionary update of the velocity, i.e.,:

$$\begin{aligned} v_{id}(t) = \omega \times v_{id}(t-1) + C_1 \times rand_1 \times \left(p_{id}^{best} - x_{id}(t) \right) \\ + C_2 \times rand_2 \times \left(p_{gd}^{best} - x_{id}(t) \right) \end{aligned} \tag{44}$$

The position update formula is the same as that of the elementary particle swarm optimization algorithm. The introduction of inertia weights ω in the velocity update formula plays a key role in equalizing the local optimal capacity and the global optimal capacity. Therefore, the inertia weight ω is generally not set as a fixed value, but as a function that decreases linearly with time transformation, and the expression can be written as:

$$\omega = \omega_{\max} - \frac{\omega_{\max} - \omega_{\min}}{k_{\max}} \cdot k \tag{45}$$

where: $\omega_{\max}$ is the initial weight, $\omega_{\min}$ is the final weight, $k_{\max}$ is the maximum number of iterations, and k is the current number of iterations;

2.4.4 Solution process

The particle swarm optimization algorithm with inertia weights is applied to solve the steps of the optimization model for the environmental effect of the hybrid PV-coal power generation system, and the solution process is shown in Fig. 12.

(1) Initialization. Read in the distribution network data, obtain the distribution network branch data and node data, calculate the initial tidal current of the distribution network, and record the values of raw network loss and voltage magnitude.

(2) Design of coding scheme. In this paper, we take advantage of the PSO algorithm's characteristics of real number coding in continuous space, and optimize the location and installation capacity of DGs accessing the distribution network at the same time. For a radial distribution network that allows N nodes to install DGs, let each DG be installed at a load node and only one DG can be installed at each node. then the installed active capacity of DGs is converted into a numerical number to represent it, which can be represented by a set of variables $P = \{P_1, P_2, ..., P_i, ..., P_N\}$, i.e., $P_i = x_i P_0$, P_0 is the baseline installed capacity, x_i is taken to be a real number between $[0, M_i]$, $M_i = (P_{DG,\max} / P_0)$, and $P_{DG,\max}$ is the maximum capacity of the system allowed to access the DG. If $x_i = 0$ means that the ith load node is not

installed with DG, and $x_i = m$ means that the active capacity of this load node is mP_0.

(3) Set the operating parameters of the particle swarm algorithm. Set the number of iterations. Set the maximum and minimum values of individual particles and speed.

(4) For each initial particle, calculate the system trend and the fitness value of the particle using the forward back generation method, and find the individual extreme value and the group extreme value according to the fitness value of the initial particle.

(5) Sort the fitness of all particles and perform crossover operation. The velocity and position of the resulting new particle population are updated.

(6) Substitute the updated particles into the trend calculation program and re-evaluate the fitness values of the particles.

(7) Determine whether the number of ground iterations has reached the maximum number of iterations, if so, end. If not reached, go to the next iteration.

(8) Output the results.

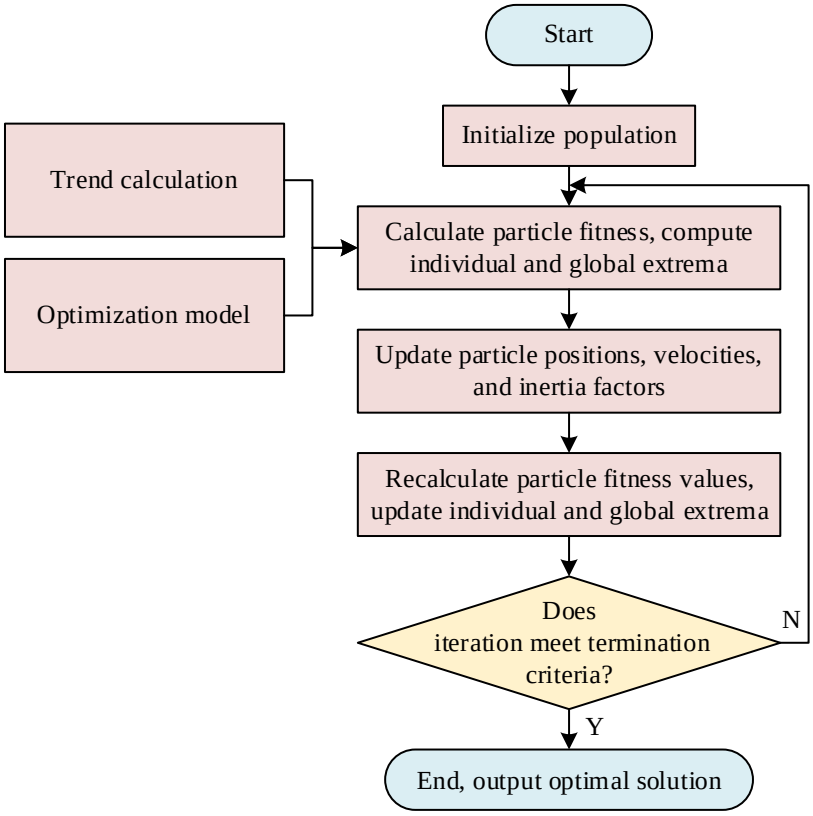

Figure 12: Optimization solution flowchart

3 Example analysis

3.1 Coal Power Generation Modeling Analysis

This section first selects Hongliulin coal as the research object for the analysis of the coal power generation model. Then, the relevant parameters of the model are determined. Subsequently, the chemical simulation software Aspen Plus is used to conduct simulation calculations for the coal power generation model. Based on the results of the model energy comparison and model exergy comparison analysis, the validity of the coal power generation model proposed in this paper is verified.

3.1.1 Parameter setting

The coal power generation model was simulated using the chemical engineering simulation software Aspen Plus, and the validity of the proposed coal power generation model was verified through energy analysis and exergy analysis. Hongliulin coal reserves are abundant. In this study, Hongliulin coal was used as the fuel for the simulation research. The physical properties of Hongliulin coal are shown in Table 1.

Table 1: The physical properties of Hongliulin coal

Elemental analysis/wt%					Industrial analysis/ wt%				LHV(MJ/kg)
Carbon	Hydrogen	Nitrogen	Sulfur	Oxygen	Moisture	Ash content	Volatile matter	Fixed carbon	
73.64	4.64	1	1.06	9.18	2.74	6.77	33.14	57.09	29.56

Checking the related information, the parameter settings are shown in Table 2. The pressure in the gasifier is 20-30MPa and the temperature is between 635-680°C, which can realize the complete carbon conversion. The gasification temperature and pressure in the simulation process of this paper are 650.04°C and 24.2MPa, respectively, the carbon conversion rate is set to 95.3%, and the coal-water slurry concentration in the gasifier is set to 20.8%. The gasifier adopts shell and tube heat exchanger, the gasification reaction is carried out in the tube side, and the flue gas goes to the shell side of the gasifier to supply heat for the gasification process, and the minimum heat transfer temperature difference in the gasifier is set to 49.4℃. The minimum heat transfer temperature difference of other heat exchangers in the model is set to 9.2℃. The isentropic efficiency and mechanical efficiency of the pump are set to 84% and 96%, respectively. The inlet temperature of gas turbine turbine can reach up to 1700℃ at the present stage, and the inlet temperature of gas turbine turbine in this paper is set to 1498℃. The isentropic and mechanical efficiencies of the compressor are set at 84% and 96%, respectively; the isentropic efficiency of the gas turbine is set at 94%. The ambient temperature and pressure are 24.3°C and 101.6 kPa, respectively.

Table 2: Parameter setting

Project	Value
Ambient temperature, ℃	24.2
Environmental pressure, kPa	101.17
Gasification temperature, ℃	650.04
Gasification pressure, MPa	24.6
Water-coal slurry concentration,%	20.8
Carbon conversion rate, %	95.3
Minimum heat exchange temperature difference of the gasifier, ℃	49.4
Pressure loss in the gasifier, %	2.7
Temperature difference at the interstitial point of the heat exchanger, ℃	9.2
Pressure loss in the waste heat boiler, %	4.7
Condensing pressure, kPa	7.8
High/low pressure of main steam, MPa	9.79/2.8
The isentropic efficiency/mechanical efficiency of the steam turbine, %	94/99.1
The isentropic efficiency/mechanical efficiency of the pump, %.	84/96
Air inlet temperature,℃	24.3
Air inlet pressure, kPa	101.6
isentropic efficiency of the compressor/mechanical efficiency, %	84/94
Turbine inlet temperature, C	1498
Transmissive entropy efficiency, %	94

The coal power generation model uses coal as fuel input and the output product is electricity. In this paper, the net generation efficiency and ï¿½efficiencyï¿½ are used to evaluate the energy utilization level of the system. The system net generation efficiency is defined in the following equation:

$$\eta_{net} = \frac{W_{GT} + W_{STUR} - W_{pump}}{m_{coal} \cdot LHV_{coal}} \tag{46}$$

where W_{GT}, W_{STUR}, W_{pump} are the gas turbine power generation, turbine power generation, and electricity consumed by all pumps, kW, respectively. m_{coal} is the mass flow rate of coal, kg/s. LHV_{coal} is the low level heat generation of coal, KJ/kg. The energy efficiency is defined as follows:

$$\eta_{ex} = \frac{E_{GT} + E_{STUR} - E_{pump}}{m_{coal} \cdot e_{coal}} \tag{47}$$

where E_{GT}, E_{STUR} and E_{pump} are the mechanical energy output from the gas engine, the mechanical energy output from the turbine, and the mechanical energy consumed by the pumps, respectively, in kW. e_{coal} is the energy per unit of mass in kJ/kg, and the chemical energy of the solid fuel is calculated by the following equation. i.e:

$$e_{coal} = LHV_{coal} \cdot \left(1.0057 + 0.1514 \cdot \frac{w_H}{w_C} + 0.0608 \cdot \frac{w_o}{w_c} + 0.0424 \cdot \frac{w_N}{w_C} \right) \tag{48}$$

3.1.2 Data analysis

Referring to the existing information, the GE-IGCC coal-based power generation model is selected as the reference model, and the energy balance of the model is calculated by simulation as shown in Table 3. At a coal consumption of 3.06 kg/s, corresponding to 92.38 MW of energy, the power generation of the reference system is 49.21 MW, of which the power generation of the gas turbine and steam turbine is 29.79 MW and 19.42 MW, respectively.The self-consumption of the reference model is 5.07 MW, which occurs mainly in the air separation unit and the syngas purification unit, with 2.51 MW and 1.39 MW, respectively.At the same amount of coal consumption, the DEH-CCS coal power generation model is able to produce the same amount of coal, and the energy balance is shown in Table 3. The same amount of coal, the DEH-CCS coal power generation model is able to produce 50.31 MW of electricity, which is 2.23% higher than the reference system. Among them, the power generation of gas turbine and steam turbine is 46.64 MW and 3.67 MW, respectively, which shows that the power generation of gas turbine in the DEH-CCS coal power generation model is much higher than that of gas turbine in the reference model, with an increase of 56.56%. The power generation of the turbine part is 3.67 MW, which is mainly due to the fact that a large portion of the exhaust heat of the gas turbine is used for gasification heat in the DEH-CCS coal power generation model.The self-consumption of power in the DEH-CCS coal power generation model is 0.23 MW, which is mainly for the feedwater pumps and the circulating pumps, and the self-consumption of power is reduced significantly by omitting the air separation unit and the syngas purification unit in the DEH-CCS coal power generation model. Finally, the net power generation reaches 50.08 MW, corresponding to a net power generation efficiency of 54.21%, which is higher than that

of the reference model by 6.43%.The gasifier loss of the DEH-CCS coal power generation model is slightly lower than that of the reference model, which is mainly due to the gasification temperature. The exhaust loss accounts for 33.97% of the energy input, which is much higher than the exhaust loss in the reference model, which is mainly due to the high water content of the flue gas, and a large portion of the heat is taken away by the flue gas in the form of latent heat of vaporization of water. The condensation loss is much lower than that in the reference model, which is mainly due to the fact that the heat to drive the Rankine cycle is greatly reduced in the model, and the corresponding condensation loss of the turbine exhaust is also greatly reduced.

Table 3: The energy balance of the model

Project	DEH-CCS		GE-IGCC	
	Value	Proportion/%	Value	Proportion/%
Coal mass flow rate, kg/s	3.06		3.06	
Energy input, MW	92.38	100	92.38	100
Net power output, MW	50.08	54.21	44.14	47.78
Power generation, MW	50.31	54.46	49.21	53.27
Gas turbine	46.64	50.48	29.79	32.25
Steam turbine	3.67	3.98	19.42	21.02
Self-consumption power, MW	0.23	0.25	5.07	5.49
Pump	0.23	0.25	0.28	0.3
Oxygen compressor			0.89	0.96
Purification unit			1.39	1.5
Air separation unit			2.51	2.72
Energy loss, MW	42.30	45.79	48.24	52.22
Gasifier	3.86	4.18	4.29	4.64
Smoke exhaust loss	31.38	33.97	6.98	7.56
Condensation loss	5.88	6.37	30.58	33.1
Mechanical loss	1.18	1.28	1.28	1.39
Purification unit			3.08	3.33
Air separation unit			2.03	2.20
Net power generation efficiency, %	54.21		47.78	

In order to further reveal the mechanism of performance enhancement of the DEH-CCS coal power generation model, find the key process of performance enhancement, and point out the direction for further enhancement of the coal power generation model, the model of this paper and the reference model were analyzed using the energy analysis, and the energy balance of the model is shown in Table 4. The total energy input to both models is 94.8 MW, and the effective energy output of DEH-CCS is 50.24 MW, which is 13.82% higher than the effective energy output of the reference model. The losses of this paper's model and the reference model are 44.56 MW and 50.63 MW, respectively.In order to further explore the parts where the losses occur, the modeled losses are divided into four panels: the fuel conversion process, the heat exchange process, the transformer process, and the other losses. The fuel conversion process mainly consists of two parts, i.e., the gasification process that occurs in the gasifier and the combustion process that occurs in the gas turbine. The hydropower loss occurring in the fuel conversion process of the DEH-CCS model is 27.36 MW, accounting for 28.86% of the total hydropower input, and the hydropower loss in this segment is lower than that of the reference model, which is 14.66%. This is mainly due to the significant reduction of the gasification

process energy loss.The heat exchanger plate energy loss in the DEH-CCS model is 2.69 MW, which is 58.99% lower than that in the reference model.The energy loss in this plate mainly includes the energy loss occurring in the syngas energy recovery unit and the energy loss occurring in the flue gas energy recovery process.There is no separate syngas energy recovery unit in the DEH-CCS model, and all the syngas energy goes to the gas turbine, avoiding the syngas energy from entering into the gas turbine, and thus the syngas energy is not used for the syngas energy recovery unit. Energy all goes to the gas turbine, avoiding 3.87 MW of heat transfer losses. Finally, the energy efficiency of the DEH-CCS coal power generation model reaches 52.99%, which is higher than that of the reference model by about 6.43%, which not only reveals the mechanism of improving the performance of the DEH-CCS coal power generation model, but also confirms the priority and validity of the DEH-CCS coal power generation model, and lays a solid theoretical foundation for the following research work to be carried out.

Table 4: Exergy equilibrium of the model

Project	DEH-CCS		GE-IGCC	
	Value	Proportion/%	Value	Proportion/%
Exergy input, MW	94.8	100	94.8	100
Exergy output, MW	50.24	53	44.14	46.56
Exergy loss, MW	44.56	47	50.66	53.44
Fuel conversion process, MW	27.36	28.86	32.06	33.82
Gasification process, MW	4.11	4.34	17.48	18.44
Combustion process, MW	23.25	24.53	14.58	15.38
Heat exchange process, MW	2.69	2.84	6.56	6.92
Energy recovery unit, MW			3.86	4.07
Waste heat boiler, MW	2.69	2.84	2.70	2.85
Work process, MW	4.68	4.94	6.09	6.42
Gas turbine	2.87	3.03	2.26	2.38
Air compressor	1.28	1.35	1.27	1.34
Steam turbine	0.27	0.28	1.46	1.54
Pump	0.26	0.27	0.07	0.07
Oxygen compressor			1.03	1.09
Other losses, MW	9.28	9.79	5.95	6.28
Exergy loss from flue gas, MW	5.04	5.32	0.32	0.34
Condensing exergy loss, MW	0.36	0.38	1.38	1.46
Throttle valve	3.88	4.09		
Syngas purification, MW			2.26	2.38
Air separation unit, MW			1.99	2.10
Exergy efficiency, %	52.99		46.56	

3.2 Modeling Analysis of Photovoltaic Power Generation

Combined with the derivation formula of the PV model above, the simulation and analysis environment of the PV model is set up in Matlab software. On the basis of setting each parameter of the PV power generation model, the actual utility of the PV power generation model is demonstrated by analyzing the results of different factors and the output curve of the PV power generation model, aiming to ensure the reliability of the subsequent hybrid power generation system.

3.2.1 Model parameters

Based on the above derivation of the PV generation model its model is constructed in Matlab, encapsulated and then simulated, Table 5 shows the various parameter settings of the PV generation model. The output characteristics of the PV model are nonlinear and are affected by environmental factors such as irradiance and temperature. In order to accurately analyze the effect of each environmental variable on the output characteristics of the PV power generation model, this paper adopts the research method based on variable control, i.e., to change the value of temperature under the condition of irradiance remains unchanged, as well as to change the value of irradiance while the temperature remains unchanged, so as to carry out the analysis.

Table 5: Parameter Settings for photovoltaic power generation models

Parameter Name	Parameter
Maximum power point	206.21W
Open-circuit voltage	36.15V
Short-circuit current	7.77A
Maximum power point voltage	29.54V
Maximum power point current	29.54A

3.2.2 Analysis of results

In order to test the effect of different irradiance on the output characteristics of the PV model, four different irradiance conditions were set, namely 585W/m², 776W/m², 991W/m² and 1162W/m², and the ambient temperature was guaranteed to be 22℃ at all times, so as to record the output characteristic curves of the PV model under the corresponding conditions.

The model I-U characteristics under irradiance variation are shown in Fig. 13. The short-circuit current of the PV model increases when the irradiance gradually increases at a constant ambient temperature. At the same time, the open-circuit voltage increases with increasing irradiance, but the increase is relatively limited, and the open-circuit voltage is almost constant with increasing irradiance.

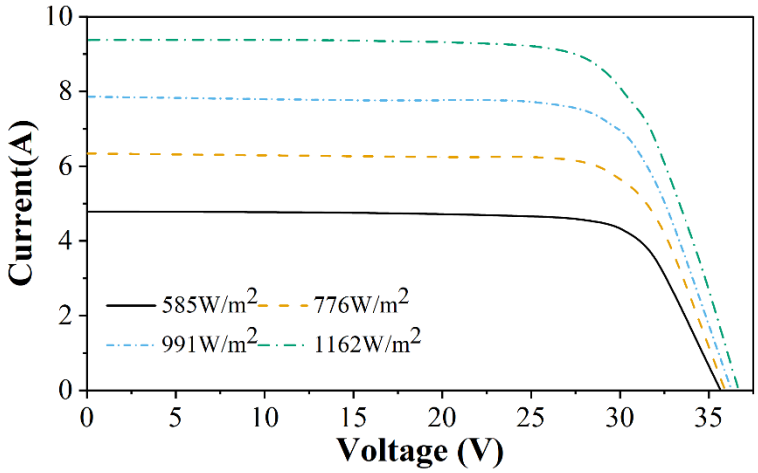

Figure 13: Model I-U characteristics under irradiance variation

The model P-U characteristics under irradiance variation are shown in Fig. 14. In terms of the P-U characteristic curve, the power value corresponding to the maximum power point increases significantly with increasing irradiance. While the increase in irradiation drives the short-circuit current to increase, the open-circuit voltage also increases, resulting in an increase

in the output power. Moreover, the voltage and current corresponding to the maximum power point also change according to the irradiance.

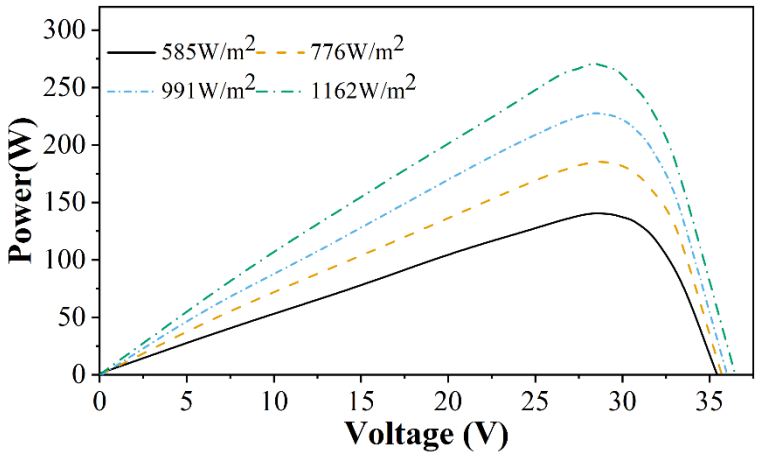

Figure 14: P-U characteristics of the model under irradiance variation

In order to test the effect of different temperatures on the output characteristics of the PV power generation model, the irradiance is set to be constant at 991W/m², while the temperatures are set to be 0°C, 25°C, 50°C and 70°C, respectively, and the output characteristics of the PV cells under the corresponding conditions are recorded, and the I-U characteristics of the model under the temperature change are shown in Fig. 15. When the irradiance is kept constant and the temperature increases, the short-circuit current of the PV model increases and the open-circuit voltage decreases with the increase in temperature.

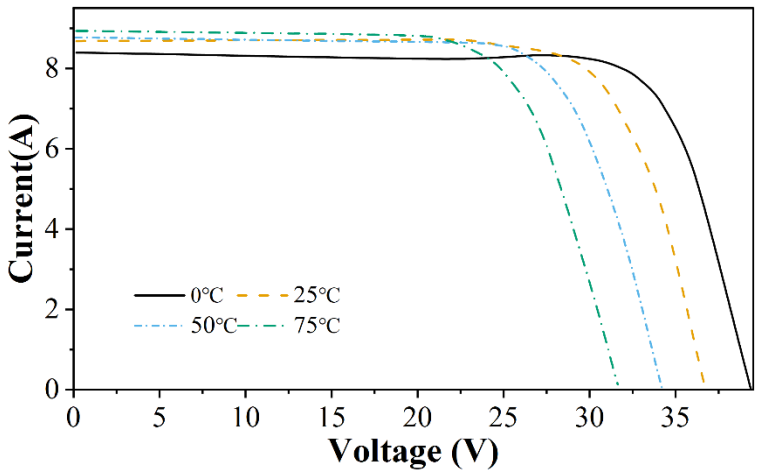

Figure 15: Model I-U characteristics under temperature variations

The P-U characteristics of the PV model under temperature variation are shown in Fig. 16. In terms of the P-U characteristic curve, an increase in temperature causes a decrease in the power value at the maximum power point, and the voltage corresponding to the maximum power point decreases This is due to the fact that power is the product of voltage and current, and a significant decrease in the open-circuit voltage leads to a decrease in power, despite the fact that there is a slight increase in the short-circuit current.

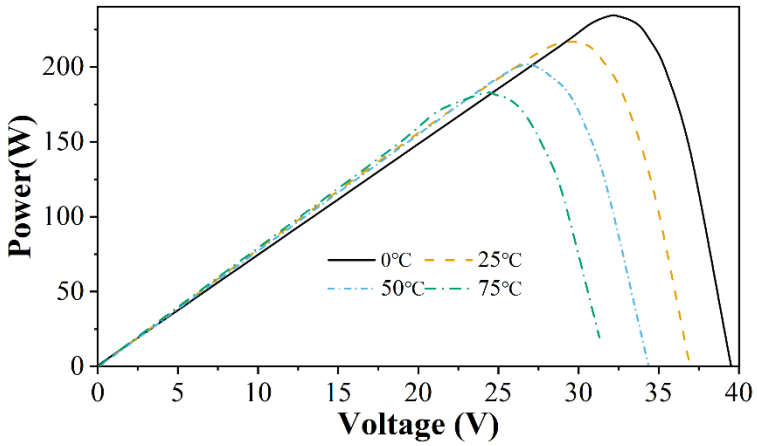

Figure 16: Model P-U characteristics

Irradiation intensity and temperature are two important factors that affect the output characteristic curve of a PV power model. The variation of irradiation intensity mainly affects the short-circuit current of the PV power model, which in turn positively affects its output power. The change of temperature has a large negative effect on the open-circuit voltage of the PV model, which indirectly affects its output power. In the actual application of PV power generation system engineering, the irradiation intensity has a greater impact on the output power of the PV power generation model, while the temperature variation has a smaller impact on the output power of the PV power generation model. The effects of different factors on the performance of the PV power generation model are demonstrated to provide theoretical support for the mathematical modeling and environmental benefit optimization of PV-coal hybrid power generation systems.

3.3 Analysis of hybrid power generation systems

Through the analysis of coal power generation model and photovoltaic power generation model, the excellent performance of the two models is understood, and then the photovoltaic-coal hybrid power generation system is constructed by combining the above research contents, and the system is explored and analyzed with the aim of proving the feasibility of the system. Under the condition of the same power generation, comparing the power generation capacity, power generation loss, power output and power generation efficiency of coal power generation system, photovoltaic power generation system and photovoltaic-coal hybrid power generation system in MW, the photovoltaic-coal hybrid power generation system is analyzed as shown in Table 6. Based on the data performance in the table, it can be seen that the power generation, power generation loss, power output, and power generation efficiency of the coal power generation system are 92.38MW, 50.08MW, 42.3MW, and 54.21%, and the power generation, power generation loss, power output, and power generation efficiency of the photovoltaic power generation system are 92.38MW, 52.72MW, 39.66MW, and 57.07%, respectively, and the two mixed The power generation capacity, power generation loss, power output and power generation efficiency of the two hybrid power generation systems are 92.38MW, 56.95MW, 35.43MW and 61.65%, i.e., it shows that the power output and power generation efficiency of the single power generation system is not as good as the hybrid power generation system, and the hybrid PV-coal power generation system is better suited to the current goal of green and sustainable development, and promotes the establishment of a low-carbon environment.

Table 6: Results of the photovoltaic-coal hybrid power generation system

Project	Coal-fired power generation system	Photovoltaic power generation system	Photovoltaic-coal hybrid power generation system
Power generation	92.38MW	92.38MW	92.38MW
Power generation loss	50.08MW	52.72MW	56.95MW
Output electrical quantity	42.3MW	39.66MW	35.43 MW
Power generation efficiency	54.21%	57.07%	61.65%

3.4 Optimization of environmental benefits of hybrid power generation systems

Through the above analysis results to obtain the power generation, power generation loss, power output, power generation efficiency of the hybrid photovoltaic-coal power generation system to provide data support for the optimization of the environmental benefits of the hybrid power generation system, before the start of the formal analysis, the performance of the improved particle swarm optimization algorithm is verified by the test function, and then only after that, the improved particle swarm optimization algorithm is used to improve the environmental benefits of the hybrid photovoltaic-coal power generation system optimization model of the The objective function is solved based on the research results to prove the validity of the research content of this paper.

3.4.1 Improved Particle Swarm Optimization Algorithm Testing

In order to verify the performance of the improved particle swarm optimization algorithm, in this section, the algorithm is tested against three typical benchmark test functions, which are Sphere test function, Rosenbrock test function, and Rastrigin test function. In this test, the position and velocity of the particles are restricted to prevent the particles from moving away from the search space. Firstly, in order to determine the size of the judgment value α, the performance of the algorithms with different values of α was tested to derive the effect of different values of α on the algorithm's performance in searching for the best. The population size in the algorithm are set to 20, the maximum number of iterations is set to 50, and the function itself is selected as the adaptation value of the algorithm. Taking the number of iterations as the horizontal coordinate and the average optimal value of each function as the vertical coordinate, the evolution curve of each function is drawn, and the evolution curve of the Sphere function is shown in Figure 17, the evolution curve of the Rosenbrock function is shown in Figure 18, and the evolution curve of the Rastrigin test function is shown in Figure 19. Comprehensive data trends in the figure can be seen, the judgment value α is too large or too small will lead to the algorithm's overall convergence speed is reduced, the stability of the algorithm is not high, and may even fall into the local optimum value of the situation. Among them, $\alpha = 0.7$ is significantly better than the other two selected values in terms of convergence speed, convergence accuracy, and stability throughout the test results.

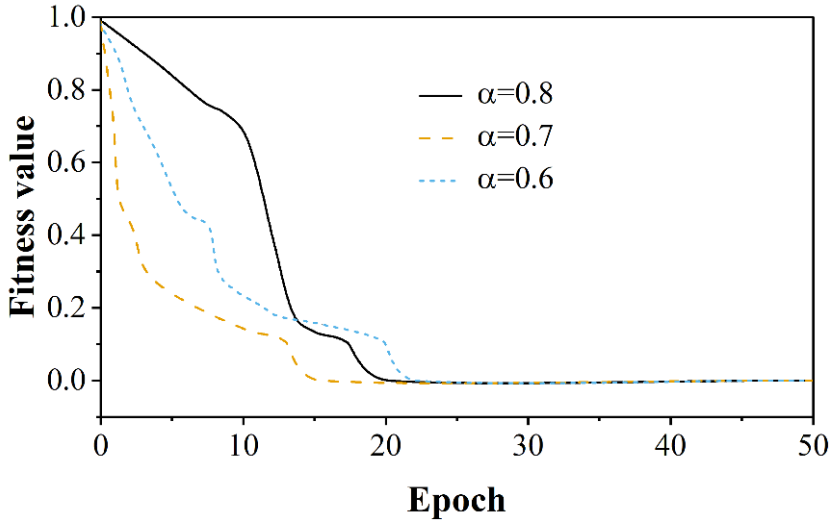

Figure 17: Evolution curve of the Sphere function

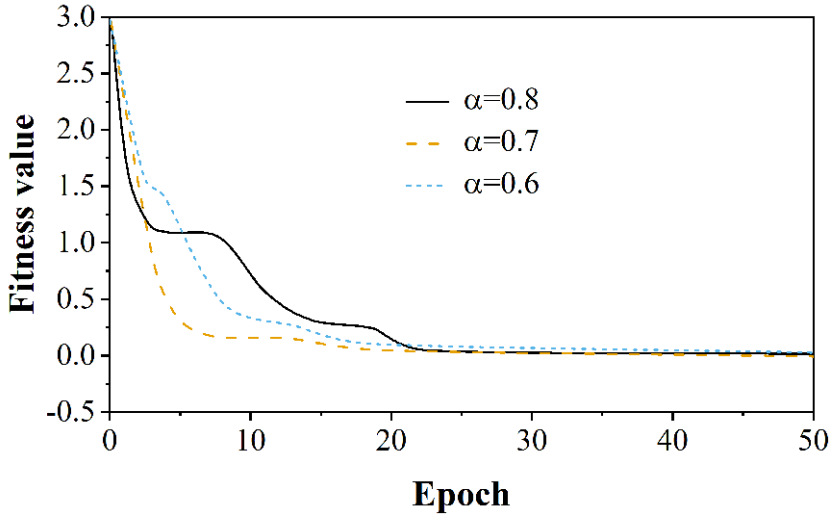

Figure 18: Evolution curve of Rosenbrock function

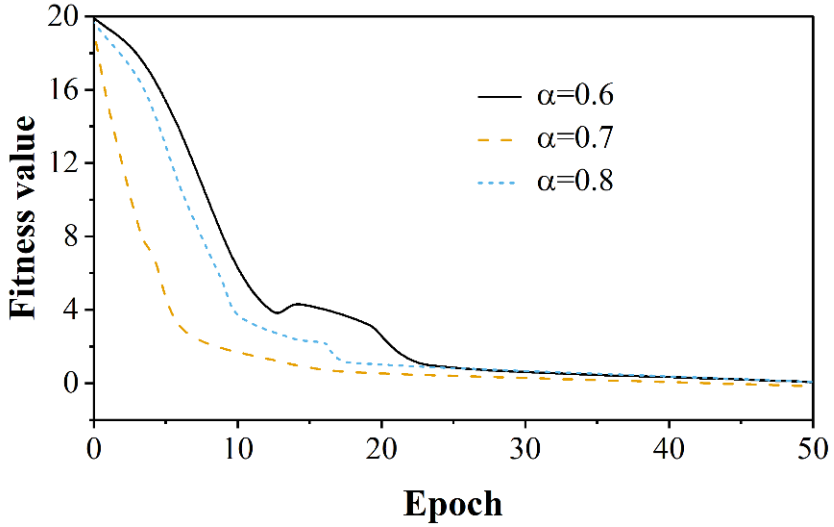

Figure 19: The evolution curve of the Rastrigin test function

In order to compare the improved PSO algorithm with the standard PSO algorithm, this paper compares the results of both tests on the benchmark test functions, and the algorithm test results are compared as shown in Table 7. According to the performance of the data in the table, it can be seen that the three functions tested with the improved PSO algorithm obtain better results than the standard PSO algorithm in terms of optimal value, number of generations of convergence and convergence rate.

Table 7: Comparison of algorithm test results

Algorithm	Function	Average optimal value	Average convergence algebra	Convergence rate
Standard PSO algorithm	Sphere	0.00000028	21	98.73%
	Rosenbrock	0.00005673	30	95.22%
	Rastrigin	0.00001848	49	77.16%
Improved PSO algorithm	Sphere	0.00000003	19	99.21%
	Rosenbrock	0.00000034	24	97.57%
	Rastrigin	0.00000017	44	92.68%

In order to analyze the change of the optimal value with the number of iterations more clearly, the convergence curve comparison graphs of three typical benchmark function test processes are given below, the convergence curve of Sphere function is shown in Fig. 20, the convergence curve of Rosenbrock function is shown in Fig. 21, and the convergence curve of Rastrigin function is shown in Fig. 22. From the convergence curve comparison diagram, it can be concluded that the improved PSO algorithm proposed in this paper is better than the standard PSO algorithm in terms of solution accuracy and convergence speed for Sphere test function, Rosenbrock test function and Rastrigin test function, which is a reliable and effective optimization algorithm, and it is suitable for applying to the optimization of the environmental benefits of the hybrid photovoltaic-coal power generation system. It is a reliable and effective optimization algorithm, which is suitable to be applied to optimize the environmental benefits of PV-coal hybrid power system.

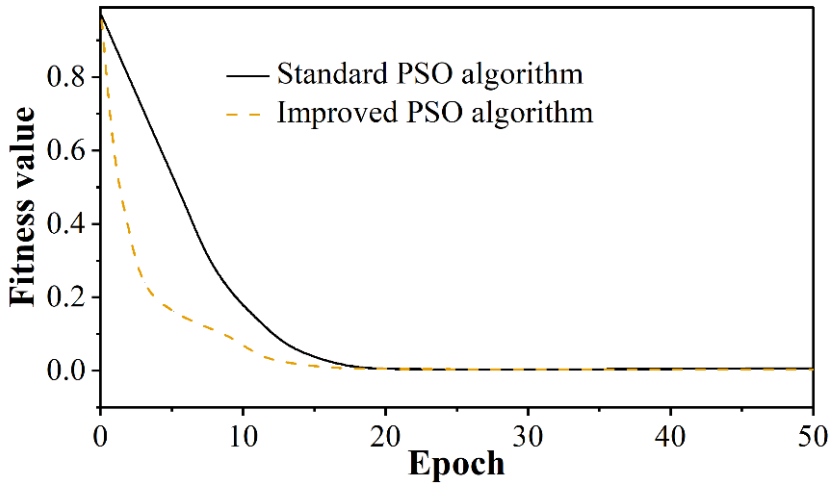

Figure 20: Convergence curve of Sphere function

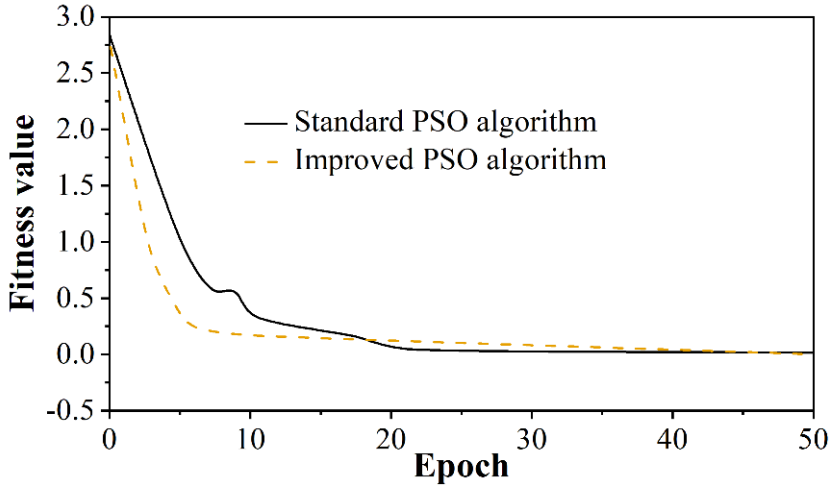

Figure 21: The convergence curve of the Rosenbrock function.

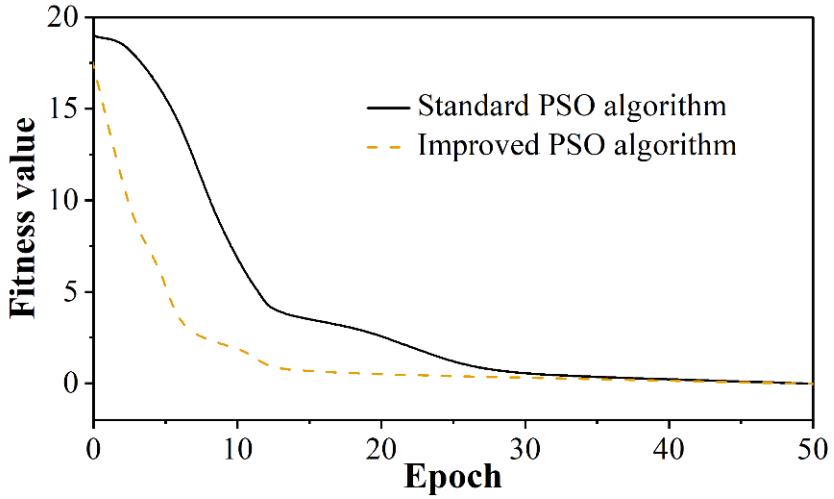

Figure 22: Convergence curve of the Rastrigin function

3.4.2 Algorithm application analysis

After verifying the effectiveness of the improved particle swarm optimization algorithm through the above three test functions, the three objective functions set above are solved and analyzed by combining the constraints and the improved particle swarm optimization algorithm, and the results of the objective functions are shown in Table 8. After the improved particle swarm optimization algorithm, the optimal solutions of investment and operation cost C_{DG}, line active loss cost C_{loss}, and environmental benefit C_{ee} of the PV-coal hybrid power generation system are 2,077,000 yuan, 23,910,000 yuan and 235,310,000 yuan, respectively, and the optimal power generation cost of the PV-coal hybrid power generation system Z is further obtained as 1.8656 million yuan. The improved particle swarm optimization algorithm can not only optimize the environmental benefit, investment and operation cost, and line active loss cost of the hybrid PV-coal power generation system, but also control the cost of the hybrid PV-coal power generation system in the optimal state, which can help the hybrid PV-coal power generation system to always implement the principle of low-carbon production.

Table 8: Objective function result

Epoch	C_{DG} /Ten thousand yuan	C_{loss} /Ten thousand yuan	C_{ee} /Ten thousand yuan	Epoch	C_{DG} /Ten thousand yuan	C_{loss} /Ten thousand yuan	C_{ee} /Ten thousand yuan
1	303.41	4.222	0.116	26	207.7	2.391	22.531
2	292.57	4.096	0.409	27	207.7	2.391	22.531
3	289.49	3.9	0.831	28	207.7	2.391	22.531
4	268.92	3.87	2.163	29	207.7	2.391	22.531
5	265.54	3.853	2.814	30	207.7	2.391	22.531
6	264.15	3.824	3.078	31	207.7	2.391	22.531
7	264.13	3.776	3.339	32	207.7	2.391	22.531
8	263.88	3.648	3.529	33	207.7	2.391	22.531
9	262.9	3.648	4.409	34	207.7	2.391	22.531
10	259.02	3.567	5.404	35	207.7	2.391	22.531
11	258.75	3.36	6.457	36	207.7	2.391	22.531
12	253.08	3.208	6.891	37	207.7	2.391	22.531
13	251.17	3.148	9.234	38	207.7	2.391	22.531
14	249.23	3.022	10.451	39	207.7	2.391	22.531
15	246.31	3.003	14.415	40	207.7	2.391	22.531
16	235.84	2.837	14.809	41	207.7	2.391	22.531
17	235.65	2.807	15.788	42	207.7	2.391	22.531
18	220.77	2.796	16.616	43	207.7	2.391	22.531
19	217.53	2.738	16.764	44	207.7	2.391	22.531
20	216.35	2.697	18.803	45	207.7	2.391	22.531
21	215.22	2.622	21.794	46	207.7	2.391	22.531
22	211.12	2.437	22.174	47	207.7	2.391	22.531
23	207.7	2.391	22.531	48	207.7	2.391	22.531
24	207.7	2.391	22.531	49	207.7	2.391	22.531
25	207.7	2.391	22.531	50	207.7	2.391	22.531

4 Conclusion

Under the background of vigorously advocating energy saving and emission reduction, green and sustainable development path, how to enhance the environmental benefits of PV-coal hybrid power generation system has become an important concern in the field of engineering. In this regard, this paper successively establishes a mathematical model of coal power generation, a mathematical model of photovoltaic power generation, and completes the design task of the hybrid photovoltaic-coal power generation system based on the combination of system identification and model downscaling. On this basis, the improved particle swarm algorithm is used to construct the PV-coal hybrid power generation system environmental benefit optimization model, and the model is analyzed by example.

(1) In the analysis of the hybrid power generation system, the output power and power generation efficiency of the single power generation system do not perform as well as the hybrid power generation system, and the output power and power generation efficiency of the hybrid power generation system have the values of 56.95MW and 61.65%, i.e., it verifies the feasibility of the PV-coal hybrid power generation system, and it has a theoretical guidance value for promoting the green and sustainable development of the power generation system.

(2) Regardless of Sphere test function, Rosenbrock test function, Rastrigin test function, the performance of the improved particle swarm optimization algorithm is greater than the standard PSO algorithm, which proves that the inertia weights can improve the local optimum and slow convergence problem of the standard particle swarm optimization algorithm. In addition, after the improved particle swarm optimization algorithm, the optimal solutions of the investment and operation cost of PV-coal hybrid power generation system, C_{DG}, line active loss cost C_{loss}, and environmental benefit C_{ee} are 2,077,000 Yuan, 23,910,000 Yuan and 235,310,000 Yuan, respectively, which not only verifies the value of the application of the optimization model of the environmental benefit of PV-coal hybrid power generation system, but also promotes the application of the optimization model of the PV-coal hybrid power generation system. It not only verifies the value of applying the optimization model of environmental benefit of PV-coal hybrid power generation system, but also promotes the green sustainable development of PV-coal hybrid power generation system.

About the Author

Ying Liu was born in Panshi, Jilin, P.R. China, in 1972. I am currently employed at CHN ENERGY JIANGSU ELECTRIC POWER GROUP CO., LTD., mainly engaged in enterprise management and legal affairs of power generation companies.

References

[1] Li, J., Zhang, Y., Tian, Y., Cheng, W., Yang, J., Xu, D., ... & Ku, A. Y. (2020). Reduction of carbon emissions from China's coal-fired power industry: Insights from the province-level data. Journal of Cleaner Production, 242, 118518.

[2] Zhang, W., Yan, Q., Yuan, J., He, G., Teng, T. L., Zhang, M., & Zeng, Y. (2020). A realistic pathway for coal-fired power in China from 2020 to 2030. Journal of Cleaner Production, 275, 122859.

[3] Zong, J., Ding, Q., Wang, H., Cao, X., & Wei, J. (2025). Analysis of the deployment scale and investment prediction of China’s coal power carbon capture technology under typical scenarios before 2050. PLoS One, 20(5), e0324240.

[4] Liu, J., Wang, K., Zou, J., & Kong, Y. (2019). The implications of coal consumption in the power sector for China’s CO2 peaking target. Applied Energy, 253, 113518.

[5] Zhang, M., Lv, T., Zhao, Y., & Pan, J. (2020). Effectiveness of clean development policies on coal-fired power generation: an empirical study in China. Environmental Science and Pollution Research, 27(13), 14654-14667.

[6] Chun, Y., Zhang, J., & Han, Y. (2023). Green development level assessment and obstacle analysis of China's coal-resource-based regions. Heliyon, 9(11).

[7] Zhang, Y. L., Kang, J. N., Liu, L. C., & Wei, Y. M. (2024). Unveiling the evolution and future prospects: A comprehensive review of low-carbon transition in the coal power industry. Applied Energy, 371, 123649.

[8] Peng, W., Wagner, F., Ramana, M. V., Zhai, H., Small, M. J., Dalin, C., ... & Mauzerall, D. L. (2018). Managing China's coal power plants to address multiple environmental objectives. Nature Sustainability, 1(11), 693-701.

[9] Gao, X., Zhao, Y., Lu, S., Chen, Q., An, T., Han, X., & Zhuo, L. (2019). Impact of coal power production on sustainable water resources management in the coal-fired power energy bases of Northern China. Applied Energy, 250, 821-833.

[10] Gao, T., Jin, P., Song, D., & Chen, B. (2022). Tracking the carbon footprint of China's coal-fired power system. Resources, Conservation and Recycling, 177, 105964.

[11] Wang, R., Cai, W., Cui, R. Y., Huang, L., Ma, W., Qi, B., ... & Wang, C. (2025). Reducing transition costs towards carbon neutrality of China's coal power plants. Nature Communications, 16(1), 241.

[12] Liu, F., & Lv, T. (2019). Assessment of geographical distribution of photovoltaic generation in China for a low carbon electricity transition. Journal of cleaner production, 212, 655-665.

[13] Liao, M., Zhang, Z., Jia, J., Xiong, J., & Han, M. (2022). Mapping China's photovoltaic power geographies: spatial-temporal evolution, provincial competition and low-carbon transition. Renewable Energy, 191, 251-260.

[14] Lei, Z., Xu, Q., Hao, G., Wei, C., & Yang, M. (2024). Voltage Coordination Control Strategy for Low Voltage Distribution Networks in Western Rural Areas under Photovoltaic Storage Access. Engineering Letters, 32(7).

[15] Wang, L., Qiu, T., Zhang, M., Cao, Q., Qin, W., Wang, S., ... & Wild, M. (2024). Carbon emissions and reduction performance of photovoltaic systems in China. Renewable and Sustainable Energy Reviews, 200, 114603.

[16] Yang, Y., Si, Z., Jia, L., Wang, P., Huang, L., Zhang, Y., & Ji, C. (2024). Whether rural rooftop photovoltaics can effectively fight the power consumption conflicts at the regional scale–A case study of Jiangsu Province. Energy and buildings, 306, 113921.

[17] Wu, C., Zhang, X. P., & Sterling, M. (2022). Solar power generation intermittency and aggregation. Scientific reports, 12(1), 1363.

[18] Pavlík, M., Beňa, L. U., Medved', D., Čonka, Z., & Kolcun, M. (2023). Analysis and evaluation of photovoltaic cell defects and their impact on electricity generation. Energies, 16(6), 2576.

[19] Guo, J., Li, R., Cai, P., Xiao, Z., Fu, H., Guo, T., ... & Song, X. (2024). Risk in solar energy: Spatio-temporal instability and extreme low-light events in China. Applied Energy, 359, 122749.

[20] Han, Y., Yan, X., Sun, Y., & Wu, J. (2025). Energy and economic analyses of a novel photovoltaic–lignite hybrid power generation system. Energy, 324, 136064.